

Published in final edited form as:

Adv Mater. 2010 February 23; 22(8): 880–885. doi:10.1002/adma.200902895.

Cooperative Nanoparticles for Tumor Detection and Photothermally Triggered Drug Delivery

Ji-Ho Park,

Materials Science and Engineering Program, Department of Chemistry and Biochemistry, University of California, San Diego, 9500 Gilman, La Jolla, CA 92093 (USA)

Geoffrey von Maltzahn,

Howard Hughes Medical Institute and Harvard-MIT Division of Health Sciences and Technology, Massachusetts Institute of Technology, 77 Massachusetts Avenue, Cambridge, MA 02139 (USA)

Luvena L. Ong,

Department of Chemical Engineering, Massachusetts Institute of Technology, 77 Massachusetts Avenue, Cambridge, MA 02139 (USA)

Dr. Andrea Centrone,

Department of Chemical Engineering, Massachusetts Institute of Technology, 77 Massachusetts Avenue, Cambridge, MA 02139 (USA)

Prof. T. Alan Hatton,

Department of Chemical Engineering, Massachusetts Institute of Technology, 77 Massachusetts Avenue, Cambridge, MA 02139 (USA)

Prof. Erkki Ruoslahti,

Burnham Institute for Medical Research at UCSB, University of California, Santa Barbara, 1105 Life Sciences Technology Bldg, Santa Barbara, CA 93106 (USA)

Prof. Sangeeta N. Bhatia, and

Howard Hughes Medical Institute and Harvard-MIT Division of Health Sciences and Technology, Massachusetts Institute of Technology, 77 Massachusetts Avenue, Cambridge, MA 02139 (USA)

Prof. Michael J. Sailor*

Materials Science and Engineering Program, Department of Chemistry and Biochemistry, University of California, San Diego, 9500 Gilman, La Jolla, CA 92093 (USA)

The ability of one structural type to perform multiple medical diagnostic or therapeutic functions is often cited as an advantageous characteristic of nanomaterials that cannot be achieved with organic small molecules.[1–3] Although there are now many examples of nanosystems that integrate multiple functions into a single structure, the designs can reduce the efficacy of the individual functions due to space and surface-chemistry limitations in the tiny platforms. For example, magnetic nanoparticles and drug molecules can be co-encapsulated in liposomes to simultaneously perform multiple functions, such as magnetic resonance imaging, magnetic drug delivery and hyperthermia,[4] but the loading capacity and the stability are typically compromised relative to a single-component liposome. There has been some effort to develop intrinsically multifunctional nanomaterials such as magnetic nanocapsules and luminescent porous silicon nanoparticles to overcome such problems,[5,6] although these more complicated structures may lose versatility in terms of the types of

*msailor@ucsd.edu.

Supporting Information is available online from Wiley InterScience or from the author.

payloads they can carry. Access to the payloads can also be limited, reducing the ability to control their release. Separating functions into two or more nanoparticle formulations is one means to simplify the problem. If two separate nanomaterials can be engineered to synergistically cooperate in their diagnostic or therapeutic functions, it is possible that the overall dosage can be reduced, minimizing side effects and providing a safer transition to the clinic.

Combination therapies are commonly employed in a wide range of cancer treatments. In particular, hyperthermia can increase the concentration of an administered therapeutic nanoparticle in a tumoral region by increasing blood flow and vessel permeability.[7,8] Hyperthermia can also enhance drug toxicity in cancer cells that are otherwise resistant to chemotherapeutics.[9] Furthermore, local hyperthermia can improve the accumulation of a drug, which is encapsulated in a thermosensitive carrier.[10,11] The combination of hyperthermia and chemotherapeutics can, therefore, be employed synergistically to treat high-risk tumors with a goal of total tumor eradication. From a clinical perspective, precise and site-specific heat transfer to a diseased site would improve the safety and efficacy of thermal cancer therapies.

Recent advances in the field of plasmonic nanomaterials have presented new opportunities for localized hyperthermia therapy. Plasmonic nanomaterials are metallic structures that efficiently convert optical radiation into heat by coupling into one or more plasmon modes.[12,13] Of particular interest are gold nanorods (GNRs) due to their large optical coefficients in the NIR region of the spectrum, where living tissue is highly transparent.[14,15] Previously, we and other groups demonstrated that GNRs can be modified to circulate for long periods of time in the blood stream and passively accumulate in tumors in vivo, where they can be heated with localized NIR radiation to selectively destroy malignant tissue regions.[16–18] In addition, the optical properties of GNRs or gold-based nanoparticles have been harnessed to image targeted tissues in vivo.[19–21] In this Communication, we hypothesized that GNRs could be used to detect a diseased site and act as tumor-specific triggers to amplify the therapeutic function of a circulating drug carrier (Fig. 1a). We find that GNR-mediated photothermal heating is highly localized in tumors and significantly improves the selectivity and efficacy of cancer treatment with thermosensitive drug carriers.

Cetyltrimethylammonium bromide (CTAB)-coated GNRs were coated with a mixed monolayer of poly(ethylene glycol) (PEG) and surface-enhanced Raman scattering (SERS)-active reporter molecules to increase circulation times, reduce in vivo toxicity, and provide remote imaging as described previously.[18,22] The gold cores appear as dark rods in the transmission electron microscopy (TEM) image (Fig. 1b), with an average width of ~13 nm and length of ~47 nm. The PEG coating is observed as a faint halo around the metal cores. The wavelength of maximum optical absorption of the GNR is 800 nm (Supporting Information, Fig. S1). As observed previously, intravenously injected PEG-coated GNRs were observed to circulate in the blood stream with a half-life of >17 h in mice, enabling passive accumulation in a xenografted MDA-MB-435 human melanoma tumor through the porous vascular structures.[18] Passive accumulation in tumors allowed tunable photothermal heating selectively in the tumor region by excitation with an 810 nm laser (Fig. 1c and Fig. S2). As has been observed with SERS-tagged gold nanoparticles,[20,22] the SERS spectrum of a surface-embedded cyanine dye on the GNRs was evident in Raman spectra obtained from the tumor in vivo (Fig. 1c and Fig. S3). Thus, the GNR formulation used in this study is an effective hyperthermia agent that can be observed in vivo with spectroscopic imaging methods.

A second nanostructure that could deliver a drug in response to the thermal stimulus from the GNRs was synthesized using a modification of published preparations.[23,24] The formulation contains thermally responsive lipid constituents chosen, in part, for their potential for translation to clinical studies. Three preparations were studied: a thermally sensitive liposome (TSL, 132.4 ± 7.2 nm hydrodynamic size), a control liposome that is not thermally sensitive (NSL, 137.1 ± 4.9 nm hydrodynamic size), and a thermally sensitive micelle (TSM, 25.9 ± 2.1 nm hydrodynamic size). All three sample types were prepared with the chemotherapeutic agent doxorubicin (DOX) in this study. The TSL displayed similar thermal properties to the published formulation.[23,25] The TSLs released ~50–60% of their drug contents in a short period of time (~30 s) when heated to 45 °C, while the nonthermally sensitive liposomes showed no significant drug release (Fig. 1d and Fig. S4). The micellar TSMs exhibited thermal sensitivity similar to that of the TSL, but they released their DOX payload more slowly at 45 °C.

We next investigated if the thermally sensitive drug carriers could deliver DOX into cancer cells at increased temperature in vitro (Fig. 2a). In the absence of drug, the cells were observed to tolerate temperatures of ~45 °C without any significant indications of toxicity. In the presence of the drug, free DOX molecules rapidly internalized into cells and bound to nuclei either with or without heating, although more DOX was observed in the nuclei of the cells heated to 45 °C. Of the three types of nanoparticles, TSLs delivered the largest quantity of DOX to cells when heated, while TSMs exhibited much lower DOX delivery. As expected, NSLs showed no temperature-induced DOX release, consistent with the lack of thermally responsive lipids in their structure. None of the three nanoparticle types displayed significant internalization of DOX into cells at 37 °C.

GNR-mediated photothermal heating significantly increased DOX-related toxicity towards cancer cells compared with control samples heated in an incubator (Fig. 2b and Fig. S5). In agreement with previous results,[9] free DOX molecules, as well as the TSMs and the TSLs, displayed slightly greater cytotoxicity at the higher temperature (45 °C) while NSLs showed no toxic effect on the timescale of the experiments. Importantly, the cytotoxicity of free DOX and TSLs was significantly enhanced when exposed to controlled GNR-mediated photothermal heating (45 °C, $P < 0.05$; Fig. 2b). The result suggests that photothermal heating by GNRs not only enhances cytotoxicity of DOX molecules, but it also induces DOX release from the heat-sensitive drug carriers, thereby, enhancing the therapeutic effect.

Consistent with the in vitro results, we found that heating of thermosensitive nanoparticles also improves drug accumulation in tumors in vivo. We first tested the ability of the thermosensitive nanoparticles to release their contents (NIR fluorescent dyes) in vivo by heating the tumoral region of the mouse with an external water bath at 45 °C (Fig. 3a and Fig. S6) Significant fluorescence intensity was observed in the heated tumors relative to the unheated control tumors. We attribute the increased nanoparticle uptake to heat-induced dilation of the vascular pores feeding the tumors. [8,10,11] Additionally, bladders from the mice injected with TSM or TSL containing a surface-attached or encapsulated fluorescent dye (TSM-VT750 and VT750@TSL, respectively) displayed strong fluorescence signals relative to the other formulations, suggesting that these fluorescent payloads are released into the blood stream selectively upon heating. However, the data indicate that TSMs are readily dissociated into free lipids in vivo at either temperature studied (Fig. S6).

Having established that application of external heat can trigger drug release in a tumor, we next tested the ability of injected GNRs to improve nanoparticle drug delivery using the laser-induced photothermal effect. The biodistribution of NSL and TSL upon photothermal heating was similar to that of other nanomaterials, with a tendency to undergo significant clearance into the mononuclear phagocyte system (MPS)-related organs (liver and spleen,

Fig. 3b).[6,20,26] However, we found that the quantity of DOX accumulated in the GNR-heated tumors was comparable to that observed in the MPS-related organs, particularly for the TSM and TSL formulations. Strikingly, the TSLs combined with GNR-mediated heating resulted in a ~12 × larger quantity of DOX accumulating in the heated tumor relative to an unheated tumor. Such a significant excess is difficult to achieve with actively targeted nanomaterials (i.e., materials containing molecular species that bind specifically to tumors or tumor-related tissues).[20,26–28] The excess can be attributed to a combination of two factors: an increase in uptake of nanoparticles through heat-dilated vessel pores and an increase in diffusion of drug out of the nanocarriers. Once free of the carrier, DOX molecules are known to bind efficiently to cancer cells in vivo.[29] TSM and NSL formulations also showed greater accumulation of DOX in GNR-heated tumors, although the quantities are statistically lower than observed for TSLs ($P < 0.05$). Free DOX molecules did not accumulate in tumors, even with GNR-mediated heating, presumably due to their short blood half-life (~5 min) and small molecular size relative to the nanoparticle carriers. The blood half-life of the liposomal and micellar formulations is much greater (~3 h), and the data illustrate the significant advantage of using encapsulants for delivery of short-lived or toxic therapeutics. Microscopic histological analysis of the tumor tissues supports the macroscopic quantitative DOX biodistribution data. Upon photothermal heating, significant quantities of DOX were observed in the extravascular region of the tumor for the TSL formulations, while DOX delivery to the tumor was somewhat limited for NSL and TSM samples (Fig. 3c).

Finally, we investigated longer-term therapeutic efficacy of the cooperative nanosystem for treatment of a human xenograft tumor in the mouse model (Fig. 4a–c). We found that the combination of GNR-mediated heating and the presence of the thermosensitive therapeutic nanoparticles significantly inhibits tumor growth without displaying significant systemic toxicity. Controls using the individual components or combinations using non- or weakly thermosensitive therapeutic nanoparticles, with or without laser irradiation, proved to be less effective.

In summary, we demonstrate that a pair of synthetic nanoparticles can work together to detect a diseased site and more effectively deliver chemotherapeutics to the site than individual nanoparticle treatments. This system relies on GNR transduction of an external optical signal into a tumor-specific thermal signal that enhances recruitment of circulating drug carriers into the tumor and triggers drug release from the carriers. GNRs localized in tumors can be identified in vivo by their intense SERS signals, making it possible to use this technology in both diagnostic and therapeutic applications. It is important to point out that non-specific uptake of the drug carriers in the MPS-related organs still remains a problem with this cooperative nanosystem, although it is significantly reduced relative to conventional therapies using single targeted drug carriers. The data presented here show that use of cooperative nanomaterials, in which each of the components has a dedicated function, can be effective at treating diseased tissues. Furthermore, it illustrates the potential advantage of dual therapeutic nanomaterials in the precision treatment of more drug-resistant cancers.

Experimental

GNR Preparation

GNRs containing a CTAB coating and displaying a peak plasmon resonance at 800 nm were purchased from Nanopartz, inc. and their CTAB coating was replaced with PEG (5kDa) molecules. To identify particles SERS, 3,3'-Diethylthiatricarbocyanine iodide molecules were trapped into the PEG coating.

Therapeutic Nanoparticle Preparation

Nonthermally sensitive DOX liposomes, thermally sensitive DOX liposomes, and DOX-loaded TSMs were prepared using a modification of published preparations [23,24]. For fluorophore conjugation (Cy7 or Alexa Fluor 488), the amine-terminated liposomes and micelles were also prepared. The prepared nanoparticles were intravenously injected in vivo to ensure that TSM, NSL, and TSL exhibited all similar circulation times (blood half-lives for all: ~3 h).

Nanoparticle Characterization

TEM images of GNRs, TSMs, NSLs, and TSLs were obtained using a Hitachi H-600A transmission electron microscope. The hydrodynamic size of GNRs, TSMs, NSLs, and TSLs was obtained using a Zetasizer ZS90 dynamic-light-scattering machine (Malvern Instruments, Worcestershire, UK).

SERS Spectral Acquisition

A Horiba Jobin Yvon Labram HR800 spectrometer was used for recording SERS spectra. Spectra were acquired with a 785-nm diode laser. In vitro SERS spectra of the cyanine-dye-tagged PEG GNRs were acquired between 100 and 1900 cm^{-1} of the Raman shift. For in vivo SERS spectra of cyanine dye-tagged PEG GNRs, 24 h after intravenous injection, in vivo Raman spectra of the anesthetized mouse were obtained in the Raman shift range 100 to 1900 cm^{-1} , using acquisition times of 30 s (liver and spleen) or 60 s (tumors and skin). The Raman laser was focused on the anatomical regions corresponding to the tumor, liver, spleen, and the skin-near tumor.

In vitro Imaging and Cytotoxicity

For fluorescence microscopy, MDA-MB-435 human melanoma cells were incubated with 80 μg DOX/mL of free DOX, TSMs, NSLs, and TSLs per well for 15 min at 37 °C or 45 °C and rinsed three times with cell medium. The cells were then incubated for an additional 1 hr at 37 °C in the presence of 10% fetal bovine serum (FBS), fixed with 4% paraformaldehyde, stained, and observed with a fluorescence microscope (Nikon, Tokyo, Japan). Cytotoxicity of the in vitro cooperative nanoystem was performed using MDA-MB-435 human melanoma cells. Cells were incubated with free DOX, TSMs, NSLs, or TSLs at different concentrations and GNRs at 7 μg Au mL^{-1} for 15 min at 37 °C or 45 °C in a cell incubator. For laser-induced (photothermal) heating, samples were irradiated for 15 min with ~0.75 W cm^{-2} of 810-nm laser light, either in the presence or absence (control) of GNRs, while maintaining an average solution temperature of ~45 °C (monitored by IR thermographic surveillance). After irradiation, the cells were rinsed three times with cell medium. The cells were then incubated for an additional 48 h at 37 °C. The cytotoxicity of free DOX, TSMs, NSLs, and TSLs was evaluated using an MTT [3-(4,5-Dimethylthiazol-2-yl)-2,5-diphenyltetrazolium bromide] assay (Invitrogen).

In vivo Behavior of Thermosensitive Nanoparticles (Laser Photothermal Heating)

First, GNRs were intravenously injected into mice bearing bilateral MDA-MB-435 human melanoma tumors (10 mg Au kg^{-1}). At 72 h post-injection, when the GNRs were completely cleared from the blood stream, therapeutic molecules or nanoparticles (5 mg DOX kg^{-1}) were systemically administered and either the right or the left flank (area where the tumor is located) was immediately irradiated with near-infrared (NIR)-light (~0.75 W cm^{-2} and 810 nm) for 30 min, maintaining the average tumor surface temperature at ~45 °C (monitored by IR thermographic observation). At 24 h post-injection of the therapeutic nanoparticles, the tissues were harvested, weighed, and homogenized to release DOX from the tissues. Following homogenization, the samples were centrifuged and supernatants of

samples were analyzed for DOX fluorescence using a fluorescence microplate reader (Molecular Devices, SpectraMax GeminiEM).

In vivo Therapeutic Studies

At 72 h post-injection of GNR (10 mg Au kg⁻¹), saline, therapeutic molecules or nanoparticles (3 mg DOX kg⁻¹) were systemically administered and one flank of the mouse (the area where the tumor is located) was either not irradiated or immediately irradiated with NIR-light (~0.75 W cm⁻² and 810 nm) for 30 min, maintaining an average tumor surface temperature of ~45 °C (monitored by IR thermographic observation). Each therapeutic cohort included ~5–7 mice. After the single treatment, tumors were measured and mice were weighed at 3 day intervals over a period of 3 weeks. All animal work was performed in accordance with the institutional animal protocol guidelines in place at the Massachusetts Institute of Technology, and it was reviewed and approved by the Institute's Animal Research Committee. Student's t-test was used for statistical analysis of the results.

A full description of the methods is available as Supporting Information.

Supplementary Material

Refer to Web version on PubMed Central for supplementary material.

Acknowledgments

This work was supported by the National Cancer Institute of the National Institutes of Health through grant numbers U54 CA 119335 (UCSD CCNE), 5-R01-CA124427 (Bioengineering Research Partnerships, BRP), and U54 CA119349 (MIT CCNE). M.J.S., S.N.B., and E.R. are members of the Moores UCSD Cancer Center and the UCSD NanoTUMOR Center under which this work was conducted and partially supported. The authors thank Edward Monosov and Luo Gu for assistance with the TEM analyses.

References

1. Park JH, von Maltzahn G, Ruoslahti E, Bhatia SN, Sailor MJ. *Angew Chem Int Ed* 2008;47:7284.
2. Weng KC, Noble CO, Papahadjopoulos-Sternberg B, Chen FF, Drummond DC, Kirpotin DB, Wang DH, Hom YK, Hann B, Park JW. *Nano Lett* 2008;8:2851. [PubMed: 18712930]
3. Wu GH, Milkhailevsky A, Khant HA, Fu C, Chiu W, Zasadzinski JA. *J Am Chem Soc* 2008;130:8175. [PubMed: 18543914]
4. Tai LA, Tsai PJ, Wang YC, Wang YJ, Lo LW, Yang CS. *Nanotechnology* 2009;20:135101. [PubMed: 19420485]
5. Piao Y, Kim J, Bin Na H, Kim D, Baek JS, Ko MK, Lee JH, Shokouhimehr M, Hyeon T. *Nat Mater* 2008;7:242. [PubMed: 18278051]
6. Park JH, Gu L, von Maltzahn G, Ruoslahti E, Bhatia SN, Sailor MJ. *Nat Mater* 2009;8:331. [PubMed: 19234444]
7. Huang SK, Stauffer PR, Hong KL, Guo JWH, Phillips TL, Huang A, Papahadjopoulos D. *Cancer Res* 1994;54:2186. [PubMed: 8174126]
8. Kong G, Dewhirst MW. *Int J Hyperthermia* 1999;15:345. [PubMed: 10519688]
9. Herman TS. *Cancer Res* 1983;43:517. [PubMed: 6184147]
10. Gaber MH, Wu NZ, Hong K, Huang SK, Dewhirst MW, Papahadjopoulos D. *Int J Radiat Oncol Biol Phys* 1996;36:1177. [PubMed: 8985041]
11. Kong G, Anyambhatla G, Petros WP, Braun RD, Colvin OM, Needham D, Dewhirst MW. *Cancer Res* 2000;60:6950. [PubMed: 11156395]
12. Hirsch LR, Stafford RJ, Bankson JA, Sershen SR, Rivera B, Price RE, Hazle JD, Halas NJ, West JL. *Proc Natl Acad Sci USA* 2003;100:13549. [PubMed: 14597719]
13. Hu M, Chen JY, Li ZY, Au L, Hartland GV, Li XD, Marquez M, Xia YN. *Chem Soc Rev* 2006;35:1084. [PubMed: 17057837]

14. Jain PK, Lee KS, El-Sayed IH, El-Sayed MA. J Phys Chem B 2006;110:7238. [PubMed: 16599493]
15. Weissleder R. Nat Biotechnol 2001;19:316. [PubMed: 11283581]
16. Niidome T, Yamagata M, Okamoto Y, Akiyama Y, Takahashi H, Kawano T, Katayama Y, Niidome Y. J Controlled Release 2006;114:343.
17. Dickerson EB, Dreaden EC, Huang X, El-Sayed IH, Chu H, Pushpanketh S, McDonald JF, El-Sayed MA. Cancer Lett 2008;269:57. [PubMed: 18541363]
18. von Maltzahn G, Park JH, Agrawal A, Bandaru NK, Das SK, Sailor MJ, Bhatia SN. Cancer Res 2009;69:3892. [PubMed: 19366797]
19. Wang HF, Huff TB, Zweifel DA, He W, Low PS, Wei A, Cheng JX. Proc Natl Acad Sci USA 2005;102:15752. [PubMed: 16239346]
20. Qian X, Peng XH, Ansari DO, Yin-Goen Q, Chen GZ, Shin DM, Yang L, Young AN, Wang MD, Nie S. Nat Biotechnol 2008;26:83. [PubMed: 18157119]
21. Song KH, Kim CH, Cobley CM, Xia YN, Wang LV. Nano Lett 2009;9:183. [PubMed: 19072058]
22. von Maltzahn G, Centrone A, Park JH, Ramanathan R, Sailor MJ, Hatton TA, Bhatia SN. Adv Mater 2009;21:3175. [PubMed: 20174478]
23. Gaber MH, Hong K, Huang SK, Papahadjopoulos D. Pharm Res 1995;12:1407. [PubMed: 8584472]
24. Tang N, Du GJ, Wang N, Liu CC, Hang HY, Liang W. J Natl Cancer Inst 2007;99:1004. [PubMed: 17596572]
25. Needham D, Anyarambhatla G, Kong G, Dewhirst MW. Cancer Res 2000;60:1197. [PubMed: 10728674]
26. Liu Z, Cai WB, He LN, Nakayama N, Chen K, Sun XM, Chen XY, Dai HJ. Nat Nanotech 2007;2:47.
27. Kirpotin DB, Drummond DC, Shao Y, Shalaby MR, Hong K, Nielsen UB, Marks JD, Benz CC, Park JW. Cancer Res 2006;66:6732. [PubMed: 16818648]
28. Weissleder R, Kelly K, Sun EY, Shtatland T, Josephson L. Nat Biotechnol 2005;23:1418. [PubMed: 16244656]
29. Cummings J, McArdle CS. Br J Cancer 1986;53:835. [PubMed: 3718837]

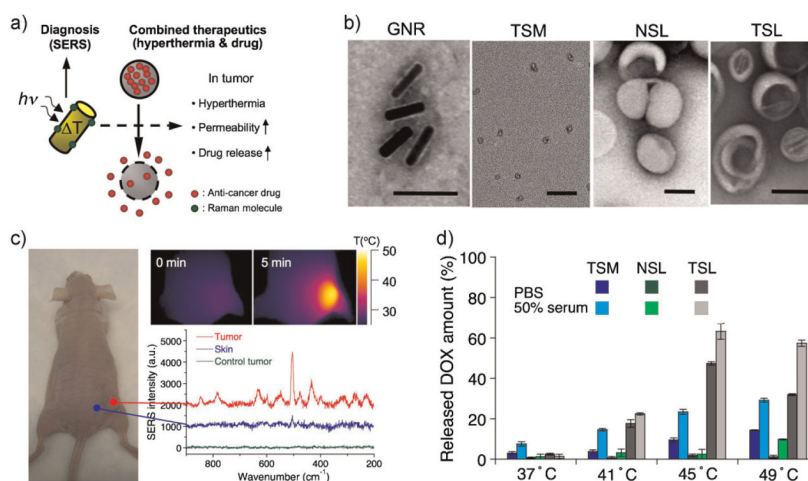


Figure 1.

Characterization of the two components of a cooperative nanosystem. a) Schematic diagram depicting the cooperative nanomaterials system. b) TEM images of PEG-coated GNR, TSM, NSL, and TSL. The scale bars are all 100 nm. c) Optical image, thermal images, and Raman spectra of a mouse depicting the multifunctionality of the GNRs. The GNRs act as thermal transducers or as SERS contrast agents when irradiated with a laser of the appropriate wavelength and intensity. The mouse, bearing a MDA-MB-435 tumor, was injected intravenously with GNRs (10 mg Au kg⁻¹). The IR thermographic maps shown were obtained 24 h post-injection; the left image was acquired immediately before and the right image 5 min after onset of irradiation with a diode laser ($\lambda = 810$ nm, 0.75 W cm⁻²). Raman spectra (5 acquisitions of 60 s each) were acquired from the tumoral region (red trace) and from skin near the tumor (blue trace). The GNRs in this experiment were labeled with a cyanine dye and the peaks in the trace correspond to the SERS spectrum cyanine dye (verified by in vitro control). d) Amount of DOX released in vitro from the liposome and micelle formulations used in this study, as a function of temperature. The samples were incubated for 10 min at the indicated temperatures and the amount of free DOX was quantified by fluorescence spectroscopy, relative to a standard curve. Values represent the mean and the error bars indicate standard deviation.

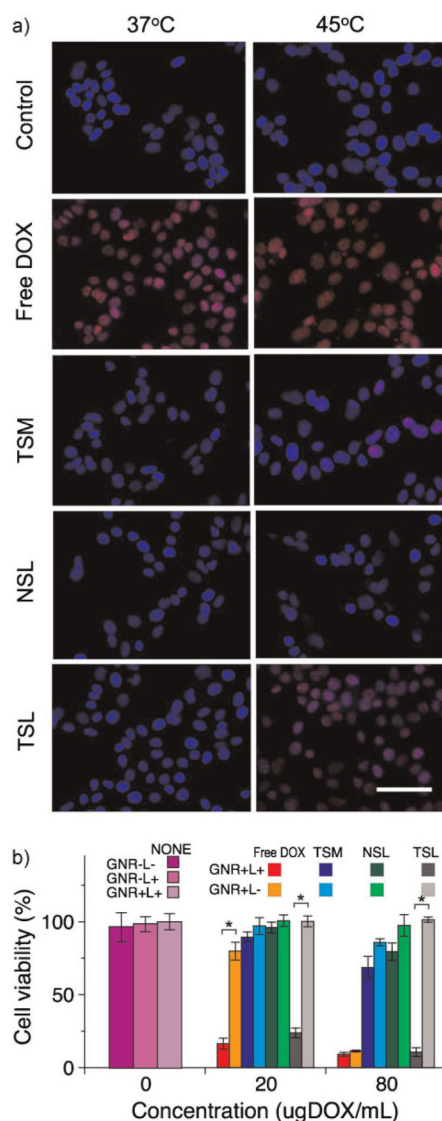


Figure 2.

Temperature-induced intracellular drug delivery and cytotoxicity of the cooperative nanosystem. a) Images showing the intracellular delivery of DOX (red) from various therapeutic nanoparticle formulations to MDA-MB-435 human melanoma cells, at two different temperatures. The cells were incubated with free DOX, TSM, NSL, and TSL for 15 min at the indicated temperatures in a cell incubator. All formulations contain $80 \mu\text{g mL}^{-1}$ of DOX. Samples were rinsed three times with cell medium, then incubated for an additional 1 h at 37°C and imaged. The nuclei were stained with 4'-6-diamidino-2-phenylindole (DAPI, blue). The scale bar indicates $100 \mu\text{m}$. b) Cytotoxicity of various photothermally activated therapeutic nanoparticle formulations to MDA-MB-435 human melanoma cells, quantified by MTT assay (* $P < 0.05$). The cells were incubated with free DOX, TSMs, NSLs, and TSLs at the indicated concentrations. GNR+ and GNR- indicate the presence or absence of GNRs ($7 \mu\text{g Au mL}^{-1}$) in the mixture, respectively. L+ and L- indicate the presence or absence of NIR irradiation (810 nm , 0.75 W cm^{-2} for 15 min), respectively. After irradiation (or 15 min in the dark for L- samples), the cells were rinsed three times with the cell-culture medium and incubated for an additional 48 h at 37°C before

administration of the MTT assay. Values represent the mean and the error bars indicate standard deviation.

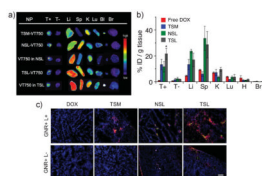


Figure 3.

Fate of thermally responsive nanostructures in vivo. a) Fluorescence images of organs from mice, where one tumor was heated at 45 °C for 30 min immediately after injection of various VT750-labeled nanoparticle formulations. The NIR-fluorescent molecular probes VT750 (750 nm excitation, 780 nm emission) were either attached to the nanoparticle surface (TSM-VT750, NSL-VT750, and TSL-VT750) or encapsulated in the internal space of nanoparticles (VT750@NSL and VT750@TSL). Mice bearing bilateral MDA-MB-435 tumors were intravenously injected with various VT750-labeled nanoparticle formulations and one tumor was immediately heated at 45 °C for 30 min in a temperature-controlled water bath. At 2 h post-injection, the tissues were collected from the mice and imaged with a NIR fluorescence imaging system. b) Biodistribution of DOX for various therapeutic nanoparticle formulations after GNR-mediated photothermal heating. Mice bearing bilateral MDA-MB-435 tumors were injected with GNRs (10 mg Au kg⁻¹). At 72 h post-injection, the indicated free DOX or therapeutic nanoparticle formulation was administered and one tumor was immediately irradiated (810 nm, ~0.75 W cm⁻²) for 30 min while maintaining an average tumor surface temperature of ~45 °C under IR thermographic surveillance. 24 h post-injection of the therapeutic nanoparticles, the tissues were collected from the mice and the native fluorescence intensity from DOX was quantified as a percentage of injected dose per tissue mass. Values represent the mean and the error bars indicate standard deviation. The differences in DOX concentration released from TSL in the heated tumor, relative to the other formulations (TSM and NSL), are significant (**P* < 0.05). c) Histological analysis of DOX distribution in MDA-MB-435 tumors treated with free DOX or the indicated therapeutic nanoparticle formulations and then subjected to GNR-mediated photothermal heating. The tissues were collected for histological analysis 6 h post-injection of the therapeutic nanoparticles (red: DOX, blue: DAPI nuclear stain, green: Alexa Fluor 488 labeled on the therapeutic nanoparticles). Abbreviations: NP, nanoparticle; T+, tumor heated to 45 °C; T-, tumor maintained at ambient temperature; Li, liver; Sp, spleen; K, kidney; Lu, lung; Bl, blood; Br, brain; H, heart. The scale bar indicates 200 μm.

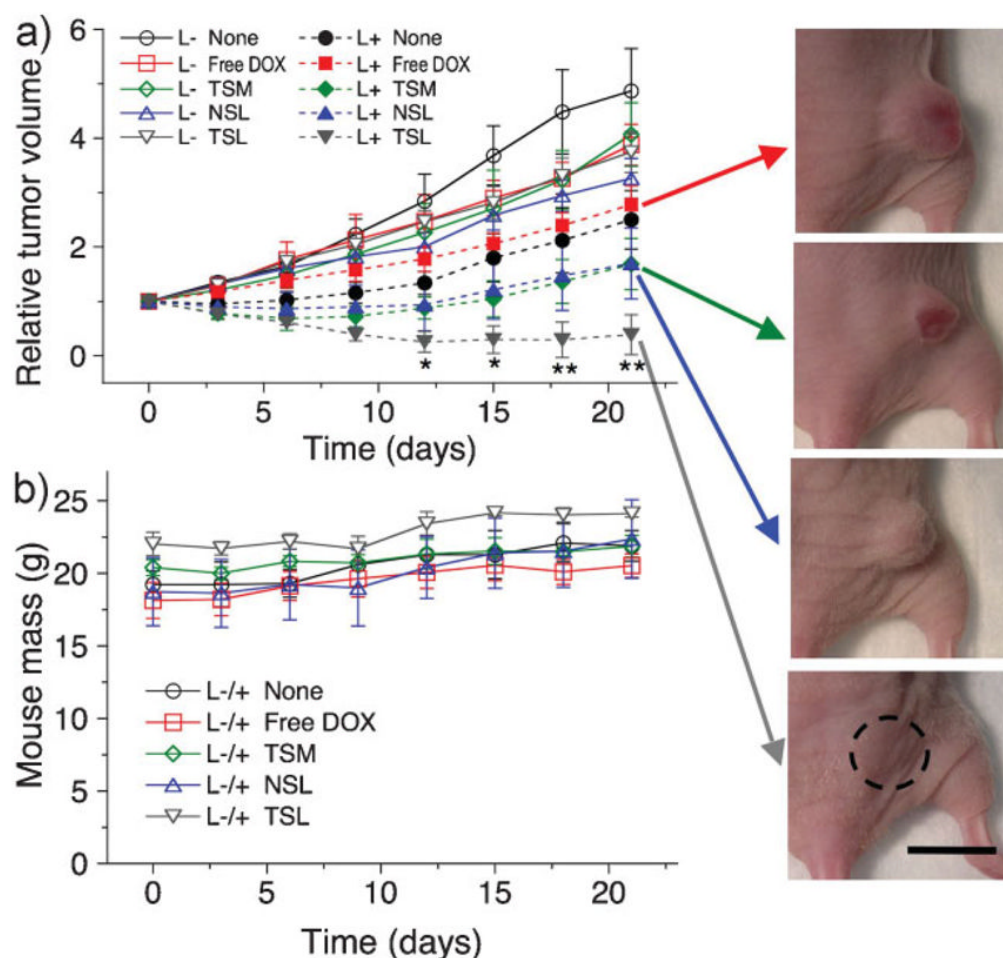


Figure 4.

Tumor therapy using cooperative nanosystem. a) Relative tumor volume in different treatment groups ($n = \sim 5-7$ mice per trace) for MDA-MB-435 human melanoma tumors. Mice bearing bilateral MDA-MB-435 tumors were injected with GNRs (10 mg Au kg^{-1}). After 72 h, a single dose of the indicated saline, free DOX, or various therapeutic nanoparticle formulations (3 mg DOX kg^{-1}) was administered through tail vein injection and one tumor was irradiated with a NIR laser (810 nm , $\sim 0.75 \text{ W cm}^{-2}$) for 30 min, while maintaining an average tumor surface temperature of $\sim 45^\circ \text{C}$ (monitored by IR thermographic surveillance). Tumor volumes were quantified every 3 d post-irradiation. The differences between TSL plus irradiation and all other groups were significant ($*P < 0.05$ for 12 and 15 days and $**P < 0.02$ for 18 and 21 days) in the tumor volume change curves. b) Representative images of treated tumors in the live animals for the indicated treatments (21 days post-treatment). Scale bar indicates 1 cm. c) Mouse mass as a function of days post-treatment for the indicated treatment groups. L+ and L- indicate animals whose tumors received NIR irradiation, or no irradiation, respectively, 72 h after GNR injection. Normal growth of all groups is observed for 3 weeks post-treatment. TSL, TSM, and NSL are the different nanoparticle formulations, defined in Figure 2.